NACA

RESEARCH MEMORANDUM

AERODYNAMICS OF SLENDER BODIES AT MACH NUMBER OF 3.12 AND REYNOLDS NUMBERS FROM 2×10^6 TO 15×10^6 V - AERODYNAMIC LOAD DISTRIBUTIONS FOR A SERIES OF FOUR BOATTAILED BODIES

By Barry Moskowitz and John R. Jack

Lewis Flight Propulsion Laboratory
Cleveland, Ohio

NATIONAL ADVISORY COMMITTEE
FOR AERONAUTICS

WASHINGTON

May 6, 1954

NATIONAL ADVISORY COMMITTEE FOR AERONAUTICS

RESEARCH MEMORANDUM

AERODYNAMICS OF SLENDER BODIES AT MACH NUMBER OF 3.12 AND REYNOLDS NUMBERS FROM 2×10^6 TO 15×10^6 V - AERODYNAMIC LOAD DISTRIBUTIONS FOR A SERIES OF FOUR BOATTAILED BODIES

By Barry Moskowitz and John R. Jack

SUMMARY

An experimental investigation to determine the aerodynamic load distributions of a series of four boattailed bodies of revolution was conducted in the NACA Lewis 1- by 1-foot supersonic wind tunnel. Pressure distributions and viscous drags were determined at a Mach number of 3.12 for a Reynolds number range of 2×10^6 to 14×10^6 and for an angle of attack range of 0° to 9°.

Significant Reynolds number effects were noted only for an increase in Reynolds number from 2×10^6 to 8×10^6 where for zero angle of attack the boattail pressure distribution level and the base pressure decreased. Varying the boattail fineness ratio from 2 to 6 resulted in a decrease in base pressure and an increase in boattail pressure distribution level.

The second-order theory of Van Dyke adequately predicted pressure distributions for all models at zero angle of attack. The hybrid theory for angle of attack yielded acceptable agreement for regions considered free of the effects of cross-flow separation, best agreement being obtained on the lower surface for small angles of attack.

INTRODUCTION

As part of a systematic program to extend the basic information on aerodynamics of bodies of revolution and to assess the validity of several theories for predicting pressures and forces acting on bodies, tests are being conducted in the NACA Lewis 1- by 1-foot supersonic wind tunnel. The first four parts of this investigation are reported in references 1 to 4. References 1 and 4 report the complete aerodynamic

characteristics of a series of four bodies having near-parabolic noses. In reference 2, the load distributions of a series of five bodies having conical or slightly blunted noses and cylindrical afterbodies are investigated. The boundary-layer development and the forces acting on a typical cone-cylinder body of revolution are reported in reference 3. Presented herein are the aerodynamic characteristics of a series of four boattailed bodies at a Mach number of 3.12 for Reynolds numbers from 2×10^6 to 14×10^6 (based on model length) and angles of attack from 0° to 9°.

Pressure distributions were obtained for all models at a Reynolds number of 14×10^6 and at Reynolds numbers of 2×10^6 to 8×10^6 for a representative model. Viscous forces were obtained for the representative model over the Reynolds number range. The experimentally determined pressure distributions for all models are compared with a second-order theory for zero angle of attack. The incremental pressure distributions due to angle of attack for the representative model are compared with a hybrid theory.

SYMBOLS

The following symbols are used in this report:

C_D	drag coefficient, $D/q_0\pi R^2$
C_P	pressure coefficient, $p-p_0/q_0$
D	drag force
d	maximum body diameter
l	length of model
l_B	length of model boattail
l_F	length of model forebody
p	static pressure
p_0	free-stream static pressure
q_0	free-stream dynamic pressure, $(1/2)\rho_0 U_0^2$
R	maximum body radius
Re	Reynolds number, $\rho_0 U_0 l/\mu$

U_0 free-stream velocity

x,r,θ cylindrical coordinates

α angle of attack, deg

μ viscosity coefficient

ρ_0 free-stream density

Subscripts:

b base

f friction

p pressure

α angle of attack

APPARATUS AND PROCEDURE

The investigation was conducted in the NACA Lewis 1- by 1-foot supersonic wind tunnel, which is a nonreturn, continuous flow, variable pressure tunnel operating at a Mach number of 3.12. Inlet pressures may be varied from 6 to 52 pounds per square inch absolute at a stagnation temperature of approximately 60° F. For the lowest pressure, the specific humidity of the air supplied to the tunnel was approximately 2×10^{-4} pounds of water per pound of dry air, thus minimizing the effect of condensation. The free-stream Reynolds number has a range of approximately 1×10^6 to 8×10^6 per foot.

Sketches of the models investigated with pertinent dimensions are presented in figure 1. The defining equations for the forebodies are

$$\frac{r}{R} = \left[2\,\frac{x}{10.5} - \left(\frac{x}{10.5}\right)^2\right]^{3/4} \quad \text{for } 0 \le x \le 10.5$$

$$\frac{r}{R} = 1 \text{ for } 10.5 \le x \le \text{ start of boattail}$$

Three of the boattails have tangent parabolic profiles defined by

$$\frac{r}{R} = 1 - \frac{1}{2}\left(\frac{x - l_F}{l_B}\right)^2$$

The fourth body has a 7.13° conical boattail of fineness ratio 2. The fineness ratio of the parabolic boattails are 6, 4, and 2 and the overall body fineness ratio is 12. The models were machined from steel and were polished to a 16-microinch finish. Each model was supported from the rear using a sting-splitter-plate mounting as shown in figure 2. There is a small effect of the splitter plate on the base pressure (see ref. 5).

Axial pressure distributions on the boattails were determined from two rows of static-pressure orifices placed 90° apart. Meridional pressure distributions were obtained for selected axial stations through orifices placed 30° apart. To keep the amount of instrumentation to a minimum, the models were instrumented in one quadrant only and then tested at both positive and negative angles of attack so that pressure distributions would be complete with respect to the meridian angle. Base pressures were determined from three static-pressure orifices placed 45° apart.

The boundary-layer data for zero angle of attack were obtained with the same probe as used in reference 3. Boundary-layer surveys were made at the start of the boattail and at the base of the model.

Reduction of Data and Method of Computation

The free-stream static pressure used in reducing the experimental data to coefficient form is that obtained from the sidewall of the tunnel opposite the model vertex position. This pressure was in close agreement with the static pressure measured on the center line of the tunnel at the same axial station. Incremental pressure coefficients due to angle of attack were obtained by subtracting the measured values at zero angle of attack from those measured at angle of attack.

The second-order theory of reference 5 as applied in reference 7 was used to obtain the theoretical pressure distributions at zero angle of attack. For angle of attack, theoretical pressure distributions were calculated using the hybrid theory suggested in reference 6 and were applied in the same manner as that given in reference 3. The hybrid theory consists of the second-order axial-flow solution of reference 6 combined with a first-order cross-flow solution of reference 8.

Skin-friction coefficients were calculated using the momentum equation in the same manner as that given in reference 1.

RESULTS AND DISCUSSION

Most of the data presented is given for the boattailed section of the bodies inasmuch as the forebody has been investigated in references 1 and 4. The experimental results obtained from the models presented in figure 1 consist mainly of pressure distributions at angles of attack from 0° to 9°. The pressure-distribution results are discussed for all models at zero angle of attack; however, because the effects of angle of attack do not vary significantly with the models, these effects are discussed only for a representative model (model 2). Also presented is the skin-friction drag at zero angle attack for the representative model.

Pressure Distributions

Zero angle of attack. - The experimental and theoretical variations of the pressure coefficient with axial station for all models at a Reynolds number of 14×10^6 and at zero angle of attack are presented in figure 3. The agreement between second-order theory of reference 6 and experiment is good for the boattailed bodies. The level of the boattail pressure distribution became less negative as the boattail fineness ratio was increased; consequently, the wave drag will decrease with increasing fineness ratio. This relation is indicated in figure 4 where the wave drag of the parobolic boattails at Reynolds number of 14×10^6 is plotted against boattail fineness ratio. Also included is the wave drag of the conical boattail which is slightly lower than the equivalent fineness-ratio parabolic boattail.

The experimental and theoretical variation of the axial pressure distribution of model 2 at zero angle of attack and for the three Reynolds numbers investigated is presented in figure 5. The agreement between second-order potential theory and experiment is good for Reynolds numbers of 8×10^6 and 14×10^6. The effect of Reynolds number is a slight decrease in pressure as the Reynolds number increases from 2×10^6 to 8×10^6.

Angle of attack. - The incremental axial pressure distributions for the representative model at angle of attack are presented in figures 6 and 7 for the bottom ($\theta = 0^\circ$) and top ($\theta = 180^\circ$), respectively, and for the Reynolds numbers investigated. Angle-of-attack data for models 1, 3, and 4 are given in table I for a Reynolds number of

14×10^6. The effect of Reynolds number is negligible except at the axial station near the base of the body. At this station, however, there appears to be no systematic Reynolds number effect.

At the bottom of the model ($\theta = 0$; fig. 6) agreement between experiment and the hybrid theory of reference 6 is good at 3° angle of attack, while at 9° the experimental increment in pressure coefficient due to angle of attack is higher than the theoretical values. This discrepancy was also noted in the investigation of the forebody of this model in references 1 and 4, and was found to change in magnitude and position as the axial location of the model was changed in the tunnel; consequently, the disagreement was attributed to a tunnel disturbance. A possible interaction between this small local tunnel disturbance and the separated cross flow might influence the pressure at θ of zero for 9° angle of attack and not have much effect at 3° angle of attack. The disagreement between theory and experiment at the top of the model (fig. 7) is attributed to the direct effects of cross-flow separation.

The experimental variation of the incremental pressure coefficient due to angle of attack with meridional angle is plotted in figure 8 at two axial stations on the boattail. At 3° angle of attack, the trends of theory and experiment are similar except near the top of the model at the 20.5-inch station where it appears that the cross flow has separated. For 9° angle of attack, the poor agreement for the bottom of the model is attributed to the tunnel disturbance mentioned previously, while the disagreement for the upper portion is primarily due to cross-flow separation.

Base Pressure

The variation of base-pressure coefficient with Reynolds number for model 2 over the angle of attack range is presented in figure 9(a). A large decrease in the base-pressure occurred between the Reynolds numbers of 2×10^6 and 8×10^6. Increasing the Reynolds number from 8×10^6 to 14×10^6 reduced the base pressure slightly at ±6° and ±9° angle of attack; however, at 0° and ±3° angle of attack the opposite trend was noted. The effect of boattail fineness ratio upon the base pressure for a Reynolds number of 14×10^6 and for the angle-of-attack range investigated is illustrated in figure 9(b). The base pressure increased with a decrease in the boattail fineness ratio. The base pressure of the conical boattailed body was slightly less negative than that of the equivalent parabolic boattailed body at the higher angles of attack, while at the low angles of attack the base pressures of the two bodies were about the same. Also presented

in figure 9(b) are the results obtained from the method of reference 9 for predicting the base pressure at zero angle of attack. Good agreement is noted only for body 3; however, the theory does predict the correct trend for the parobolic boattails.

Friction Drag

In order to complete the investigation of the component drag forces contributing to the total drag of the representative boattailed body, friction-drag coefficients were obtained from the experimentally determined displacement and momentum thicknesses at the start and at the base of the boattail. The experimental mean friction-drag coefficients for the entire body, based on maximum cross-sectional area, are presented in figure 10 for the range of free-stream Reynolds numbers investigated. Increasing the Reynolds number from 2×10^6 to 14×10^6 resulted in a decrease in skin friction until a transition Reynolds number of approximately 6×10^6 is reached whereupon the skin friction increased. To illustrate the effect of boattail on the skin friction, the data for a zero boattailed body (ref. 1) having an identical forebody is presented along with the theoretical flat-plate laminar and turbulent skin-friction coefficients. The skin friction is less for the boattailed model than the zero boattailed model. This difference is probably due to the boattailed model having less surface area than the model of reference 1.

The contribution of the various component drags to the total drag for the representative model at zero angle of attack and at Reynolds numbers from 2×10^6 to 14×10^6 is presented in figure 11. At a Reynolds number of 14×10^6, the pressure drag accounted for 51 percent of the total drag, the base drag accounted for 13 percent, and the friction drag accounted for 36 percent. The total drag of the zero boattailed body of revolution of reference 1 is about twice the total drag of the representative boattailed model; thus pointing out the value of boattailing to obtain a drag reduction.

SUMMARY OF RESULTS

The aerodynamic load distributions of four boattailed bodies of revolution were investigated in the NACA Lewis 1- by 1-foot variable Reynolds number tunnel at a Mach number of 3.12. The results may be summarized as follows:

1. At zero angle of attack, increasing the Reynolds number from 2×10^6 to 8×10^6 resulted in a slight decrease in the boattail pressure

distribution level and a large decrease in the base pressure. No significant Reynolds number effects were noted from 8×10^6 to 14×10^6.

2. Increasing the boattail-fineness ratio for the parabolic boattails resulted in a more negative value of the base pressure, and a less negative level of the boattail pressure distribution.

3. For the conical boattail at zero angle of attack, the wave drag was slightly lower and the base pressure was slightly less negative than an equivalent fineness-ratio parabolic boattail.

3216

4. The second-order theory of Van Dyke adequately predicted pressure distributions for all models at zero angle of attack. The hybrid theory for angle of attack yielded acceptable agreement for regions considered free of the effects of cross-flow separation, best agreement being obtained on the lower surface for small angles of attack.

Lewis Flight Propulsion Laboratory
National Advisory Committee for Aeronautics
Cleveland, Ohio, February 24, 1954

REFERENCES

1. Jack, John R., and Burgess, Warren C.: Aerodynamics of Slender Bodies at Mach Number of 3.12 and Reynolds Numbers from 2×10^6 to 15×10^6. I - Body of Revolution with Near-Parabolic Forebody and Cylindrical Afterbody. NACA RM E51H13, 1951.

2. Jack, John R., and Gould, Lawrence I.: Aerodynamics of Slender Bodies at Mach Number of 3.12 and Reynolds Numbers from 2×10^6 to 15×10^6. II - Aerodynamic Load Distributions of Series of Five Bodies Having Conical Noses and Cylindrical Afterbodies. NACA RM E52C10, 1952.

3. Jack, John R.: Aerodynamics of Slender Bodies at Mach Number of 3.12 and Reynolds Numbers from 2×10^6 to 15×10^6. III - Boundary Layer and Force Measurements on Slender Cone-Cylinder Body of Revolution. NACA RM E53B03, 1953.

4. Jack, John R., and Moskowitz, Barry: Aerodynamics of Slender Bodies at Mach Number of 3.12 and Reynolds Numbers from 2×10^6 to 15×10^6. IV - Aerodynamic Characteristics of Series of Four Bodies Having Near-Parabolic Noses and Cylindrical Afterbodies. NACA RM E53J27, 1954.

5. Baughman, L. Eugene, and Jack, John R.: Experimental Investigation of the Effects of Support Interference on the Pressure Distribution of a Body of Revolution at a Mach Number of 3.12 and Reynolds Numbers from 2×10^6 to 14×10^6. NACA RM E53E28, 1953.

6. Van Dyke, Milton D.: First- and Second-Order Theory of Supersonic Flow Past Bodies of Revolution. Jour. Aero. Sci., vol. 18, no. 3, Mar. 1951, pp. 161-178.

7. Van Dyke, Milton D.: Practical Calculation of Second-Order Supersonic Flow Past Nonlifting Bodies of Revolution. NACA TN 2744, 1952.

8. Tsien, Hsue-Shen: Supersonic Flow Over an Inclined Body of Revolution. Jour. Aero. Sci., vol. 5, no. 12, Oct. 1938, pp. 480-483.

9. Cortright, Edgar M., Jr., and Schroeder, Albert H.: Investigation at Mach Number 1.91 of Side and Base Pressure Distributions Over Conical Boattails Without and With Jet Flow Issuing from Base. NACA RM E51F26, 1951.

10. Tucker, Maurice: Approximate Turbulent Boundary-Layer Development in Plane Compressible Flow Along Thermally Insulated Surfaces with Application to Supersonic-Tunnel Contour Correction. NACA TN 2045, 1950.

11. von Kármán, Th., and Tsien, H. S.: Boundary Layer in Compressible Fluids. Jour. Aero. Sci., vol. 5, no. 6, April 1938, pp. 227-232.

TABLE I. - PRESSURE COEFFICIENTS FOR MODELS 1, 3, AND 4 FOR TWO ANGLES OF ATTACK AND REYNOLDS NUMBER OF 14×10^6

(a) Model 1.

Angle of attack, $\alpha = 3^\circ$								Angle of attack, $\alpha = 9^\circ$							
Axial station, x, in.	Meridian angle, θ, deg							Axial station, x, in.	Meridian angle, θ, deg						
	0	30	60	90	120	150	180		0	30	60	90	120	150	180
11	-0.006	-0.011	-0.018	-0.021	-0.022	-0.018	-0.018	11	0.032	-0.014	-0.027	-0.075	-0.053	-0.047	-0.028
13.375	-.017	------	------	-.022	------	------	-.019	13.375	.019	------	------	-.077	------	------	-.028
15.75	-.027	-.028	-.031	-.027	-.023	-.021	-.019	15.75	-.001	-.015	-.054	-.060	-.052	-.070	-.057
18.125	-.032	------	------	-.030	------	------	-.019	18.125	-.021	------	------	-.045	------	------	-.060
20.5	-.035	-.034	-.029	-.027	-.025	-.020	-.020	20.5	-.056	-.048	-.049	-.040	-.042	-.042	-.050

(b) Model 3.

Angle of attack, $\alpha = 3^\circ$								Angle of attack, $\alpha = 9^\circ$							
Axial station, x, in.	Meridian angle, θ, deg							Axial station, x, in.	Meridian angle, θ, deg						
	0	30	60	90	120	150	180		0	30	60	90	120	150	180
18	-0.024	-0.024	-0.050	-0.051	-0.026	-0.019	-0.019	18	0.000	-0.008	-0.053	-0.069	-0.061	-0.068	-0.040
19	-.062	------	------	-.058	------	------	-.045	19	-.058	------	------	-.074	------	------	-.077
20	-.075	-.076	-.075	-.070	-.062	-.061	-.061	20	-.070	-.079	-.097	-.082	-.075	-.081	-.099
20.5	-.083	------	------	-.071	------	------	-.064	20.5	-.094	------	------	-.086	------	------	-.088

(c) Model 4.

Angle of attack, $\alpha = 3^\circ$								Angle of attack, $\alpha = 9^\circ$							
Axial station, x, in.	Meridian angle, θ, deg							Axial station, x, in.	Meridian angle, θ, deg						
	0	30	60	90	120	150	180		0	30	60	90	120	150	180
18	-0.063	-0.063	-0.066	-0.065	-0.056	-0.049	-0.049	18	-0.050	-0.056	-0.087	-0.089	-0.072	-0.066	-0.061
19	-.058	------	------	------	------	------	-.048	19	-.046	------	------	------	------	------	-.066
20	-.057	-.056	-.054	-.046	-.042	-.059	-.059	20	-.052	-.063	-.076	-.057	-.059	-.060	-.066
20.5	-.055	------	------	-.040	------	------	-.053	20.5	-.055	------	------	-.052	------	------	-.057

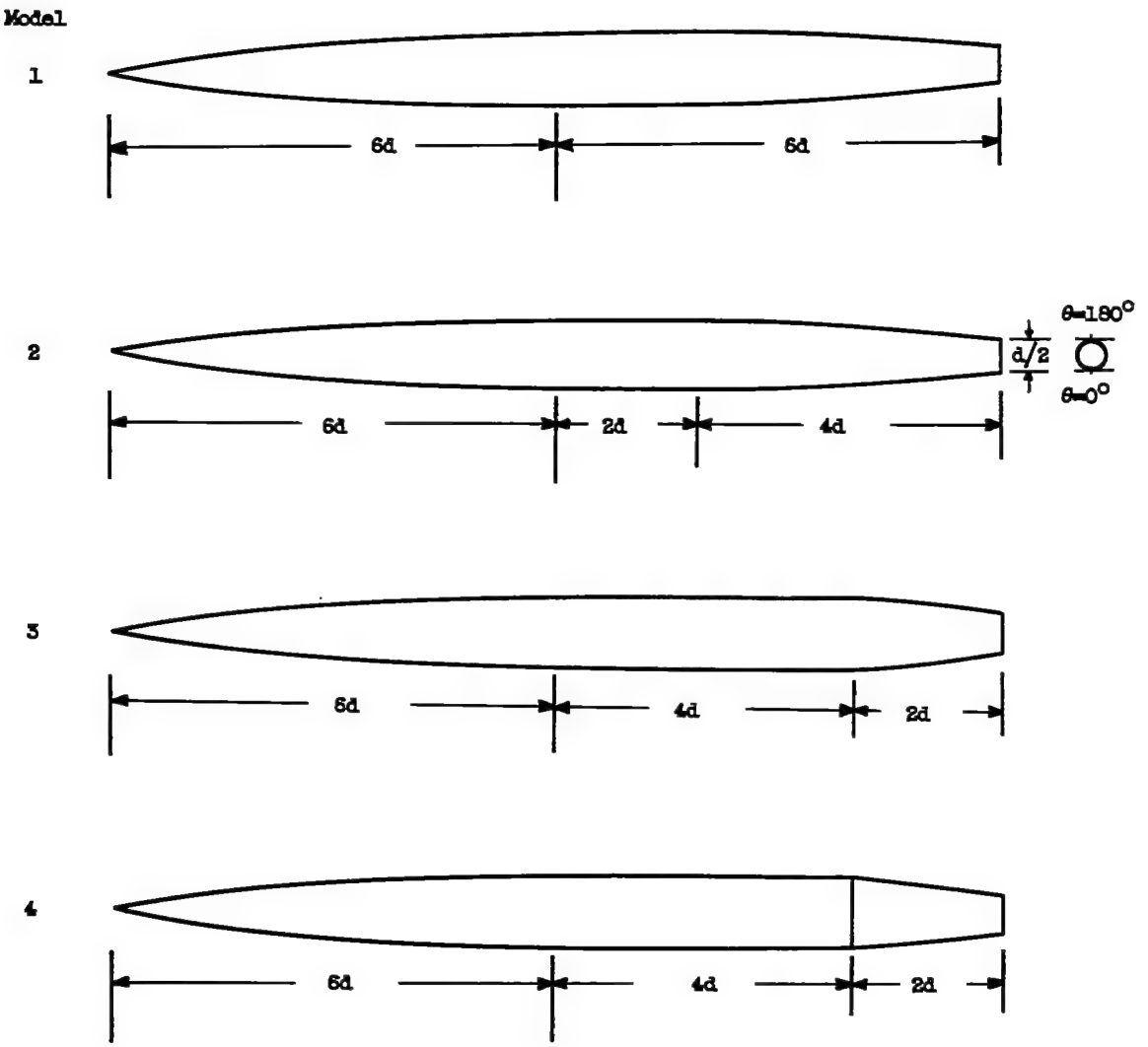

Figure 1. - Schematic drawing of models. Maximum body diameter d, 1.75 inches.

CD-2 back

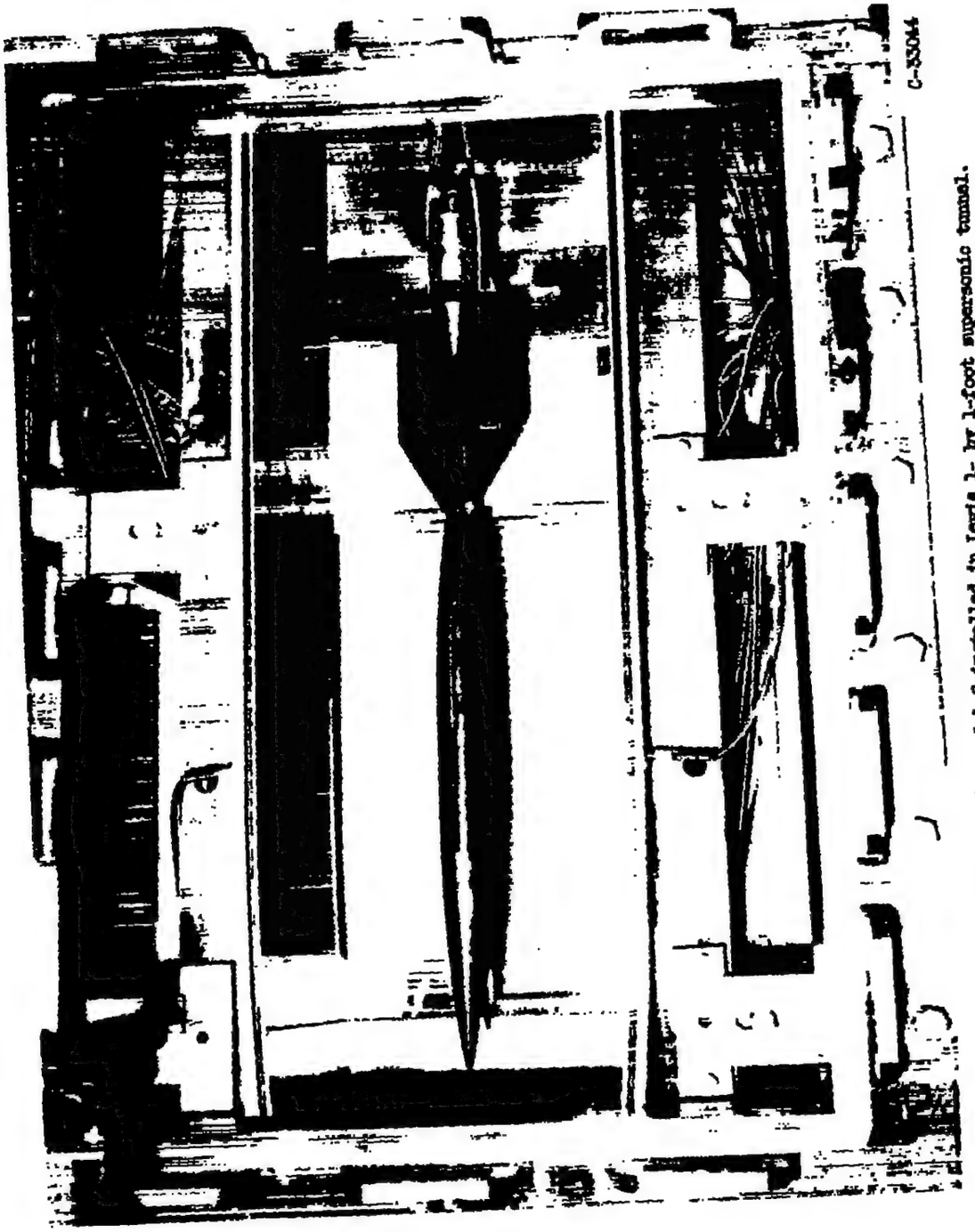

Figure 2. - Representative model 2 installed in Lewis 1- by 1-foot supersonic tunnel.

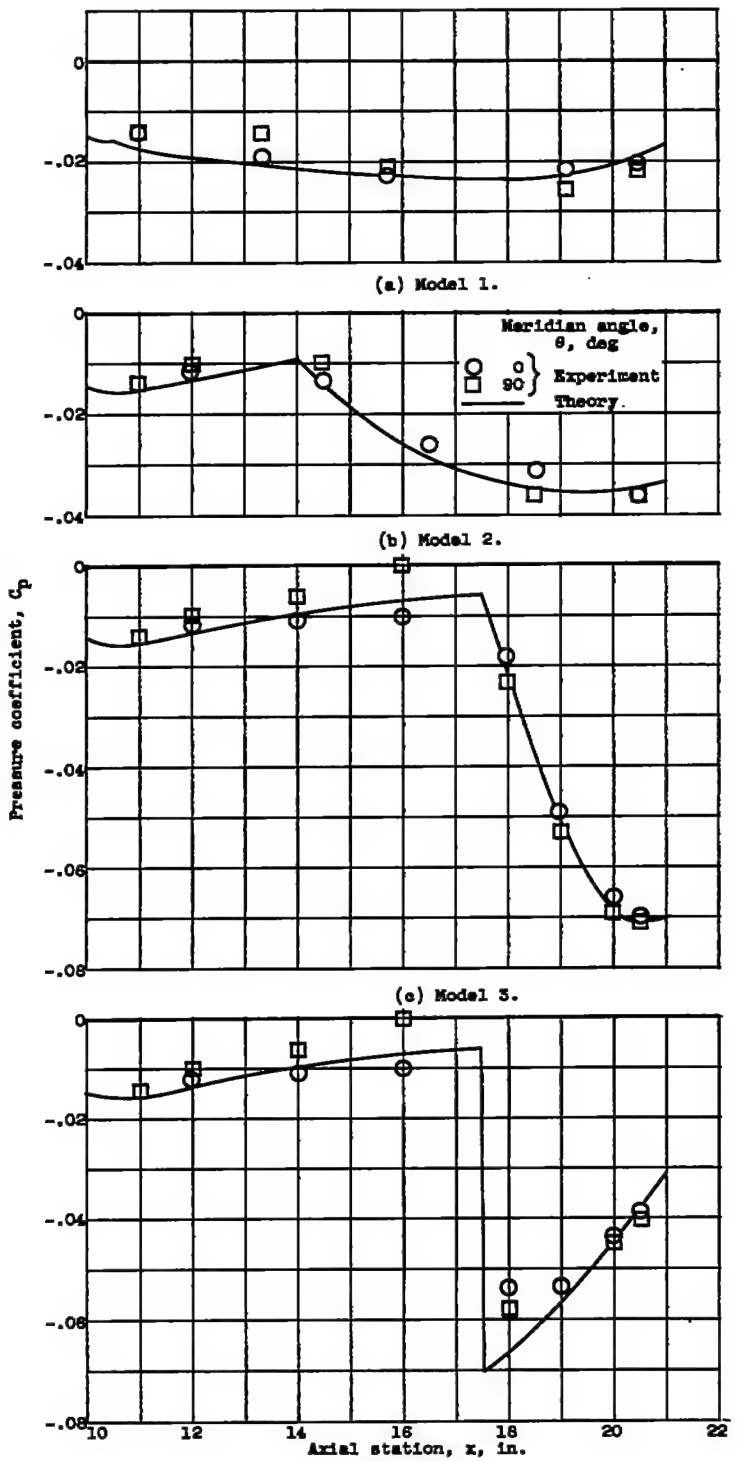

Figure 3. - Effect of boattail geometry on axial pressure distribution at zero angle of attack and Reynolds number of 14×10^6.

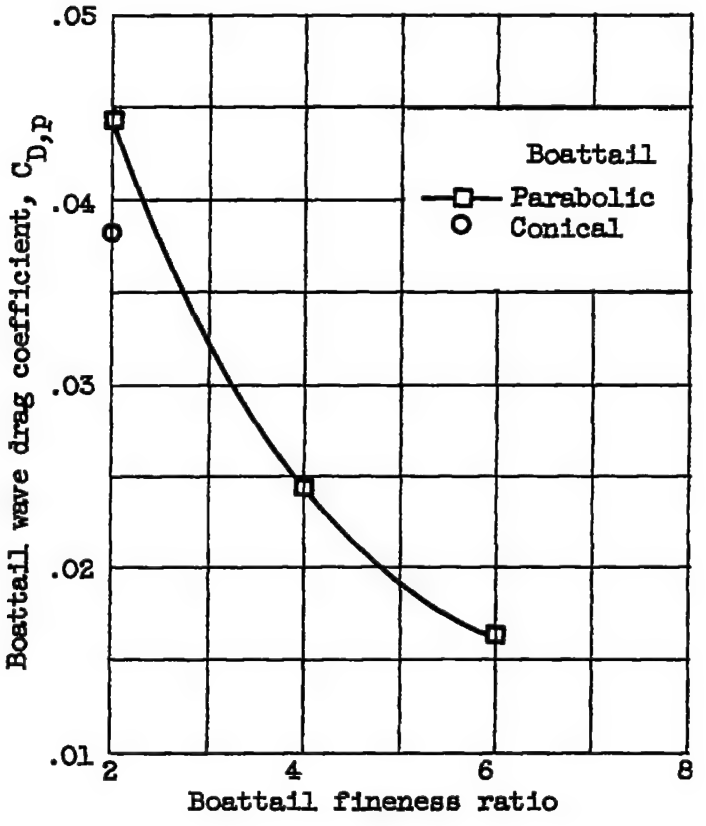

Figure 4. - Effect of boattail fineness ratio on boattail wave drag at zero angle of attack and Reynolds number of 14×10^6.

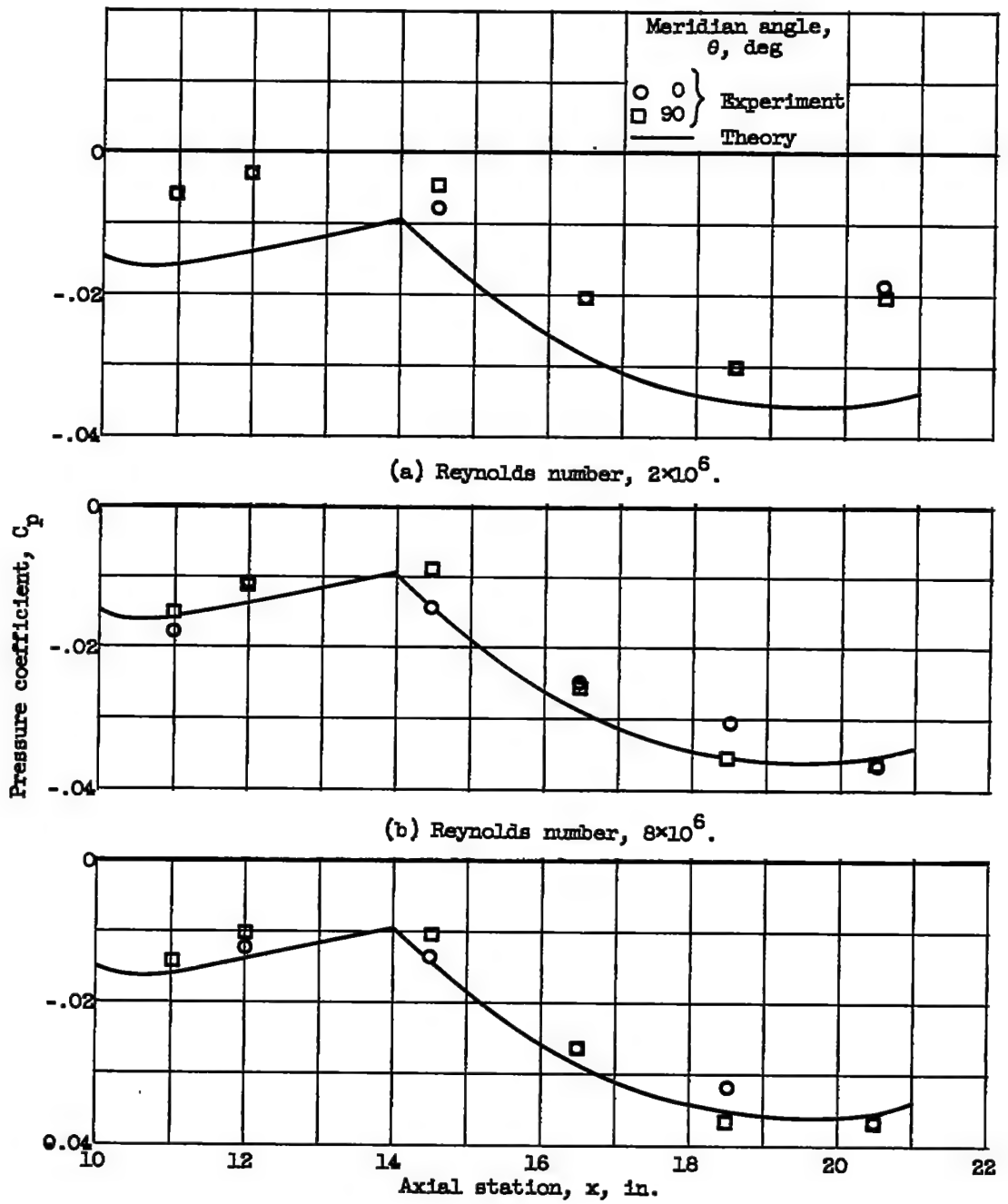

(a) Reynolds number, 2×10^6.

(b) Reynolds number, 8×10^6.

(c) Reynolds number, 14×10^6.

Figure 5. - Effect of Reynolds number on boattail pressure distribution for model 2 at zero angle of attack.

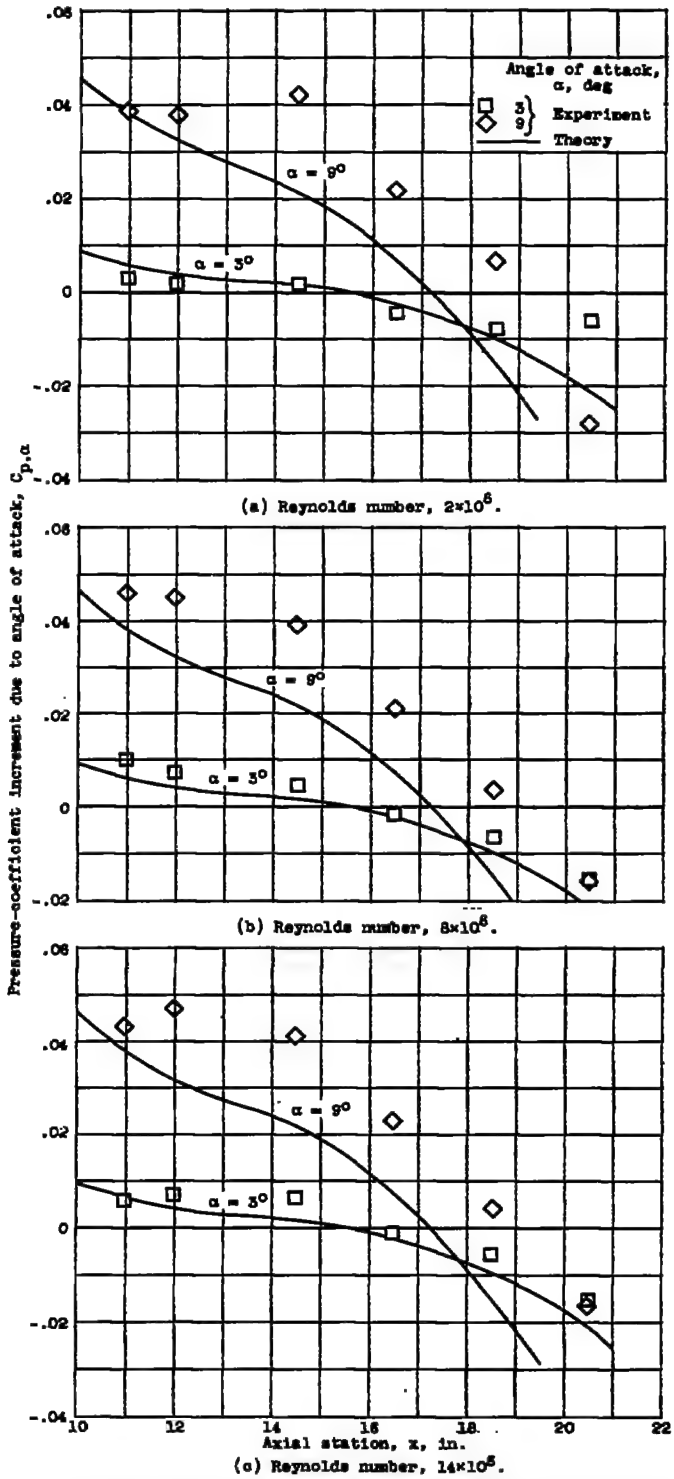

(a) Reynolds number, 2×10^6.

(b) Reynolds number, 8×10^6.

(c) Reynolds number, 14×10^6.

Figure 6. - Effect of Reynolds number on bottom-surface pressure distribution of model 2 for two angles of attack; meridian angle, zero.

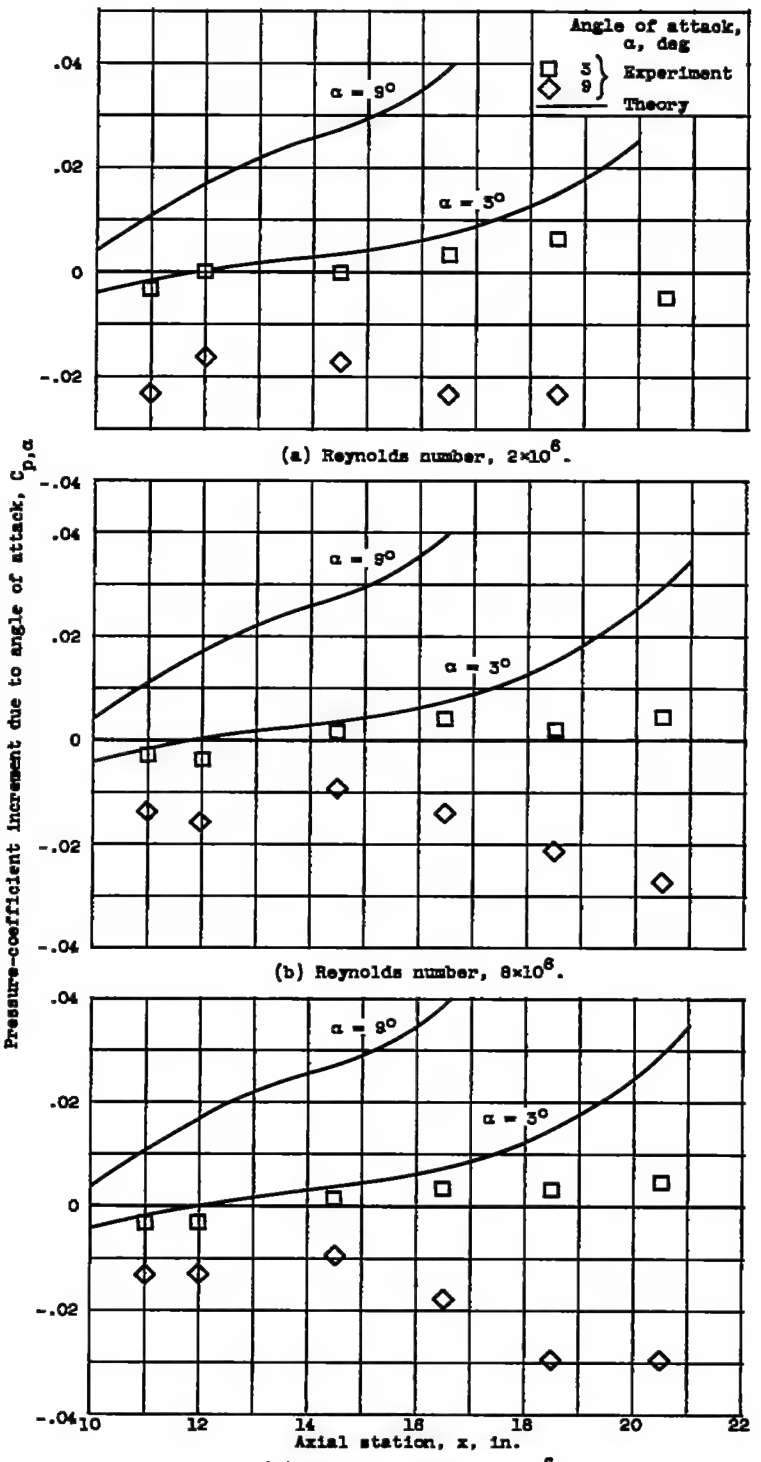

(a) Reynolds number, 2×10^6.

(b) Reynolds number, 8×10^6.

(c) Reynolds number, 14×10^6.

Figure 7. - Effect of Reynolds number on top surface pressure distribution of model 2 for two angles of attack, meridian angle, 180°.

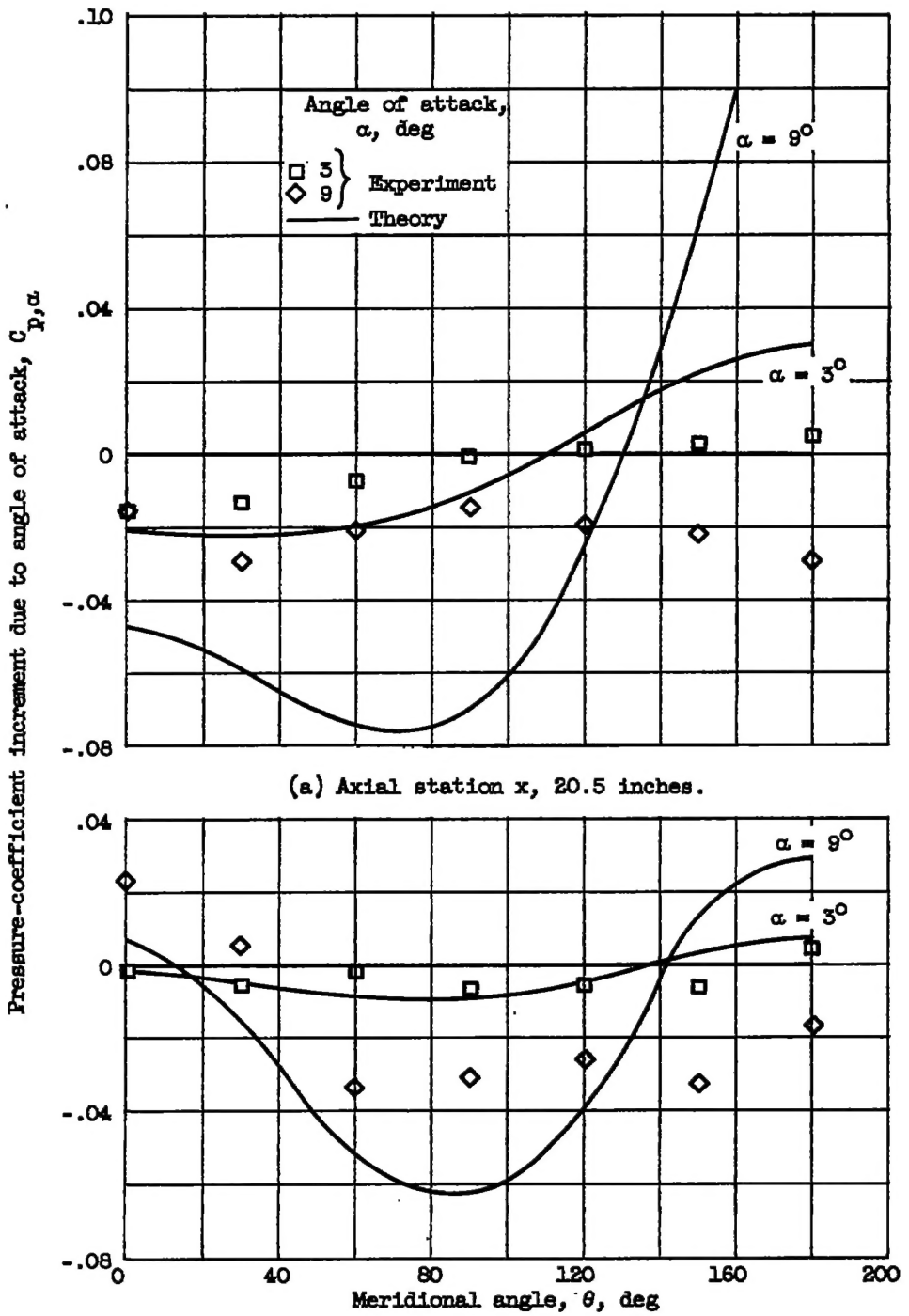

Figure 8. - Meridional pressure distribution due to angle of attack for boattail of model 2 at Reynolds number of 14×10^6.

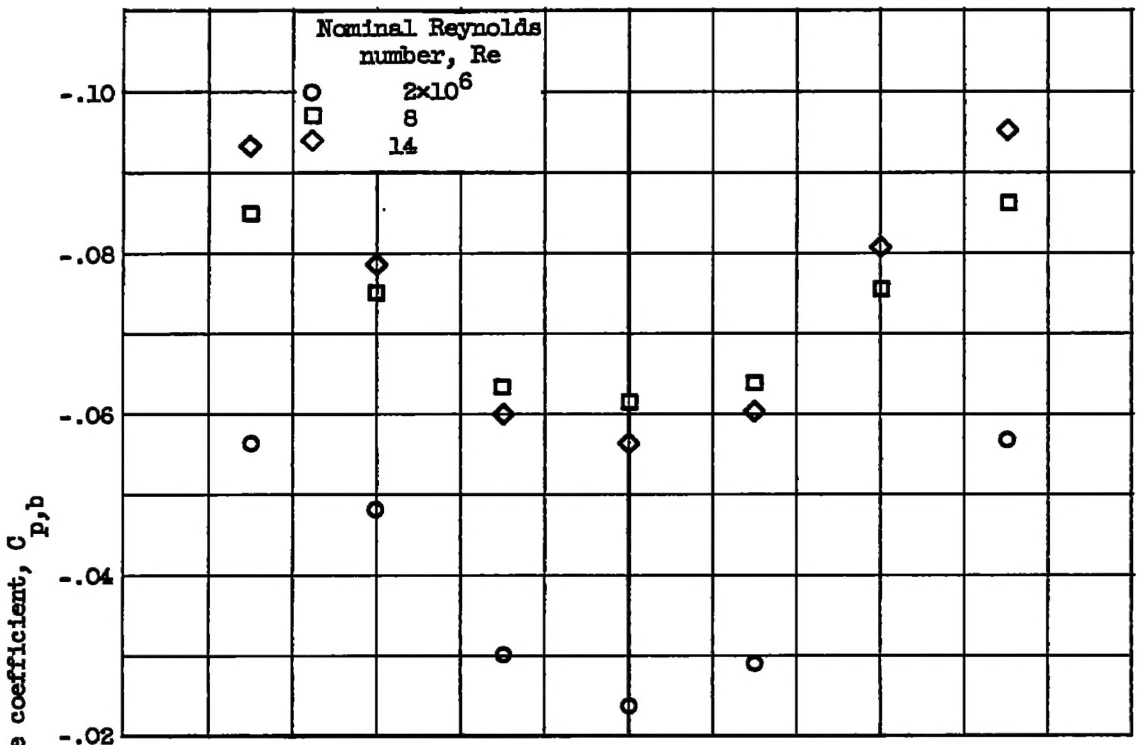

(a) Model 2.

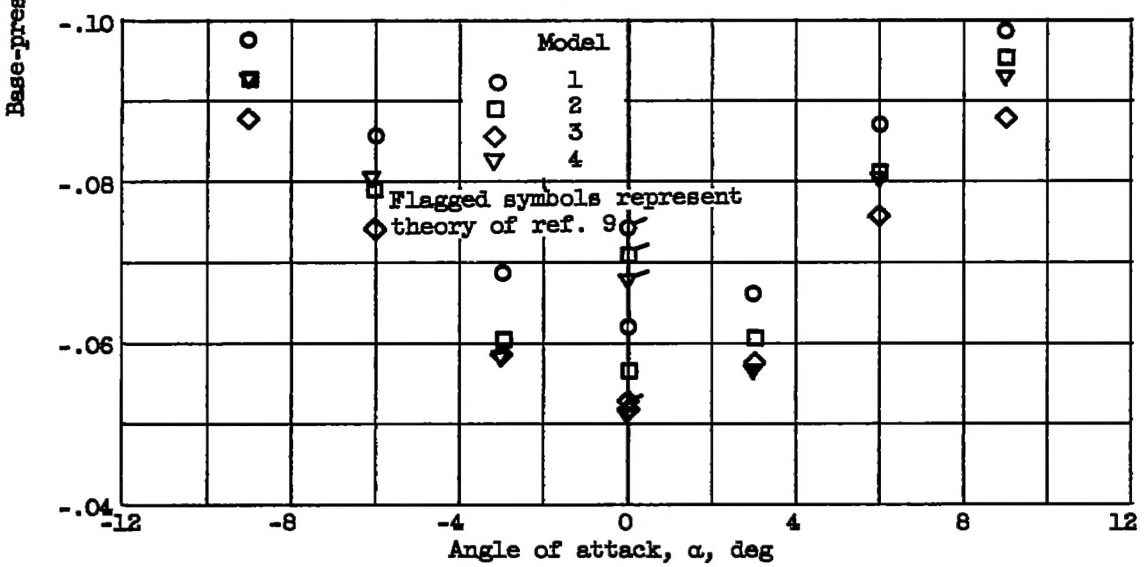

(b) Reynolds number, 14×10^6.

Figure 9. - Variation of base-pressure coefficient with Reynolds number and boattail-fineness ratio.

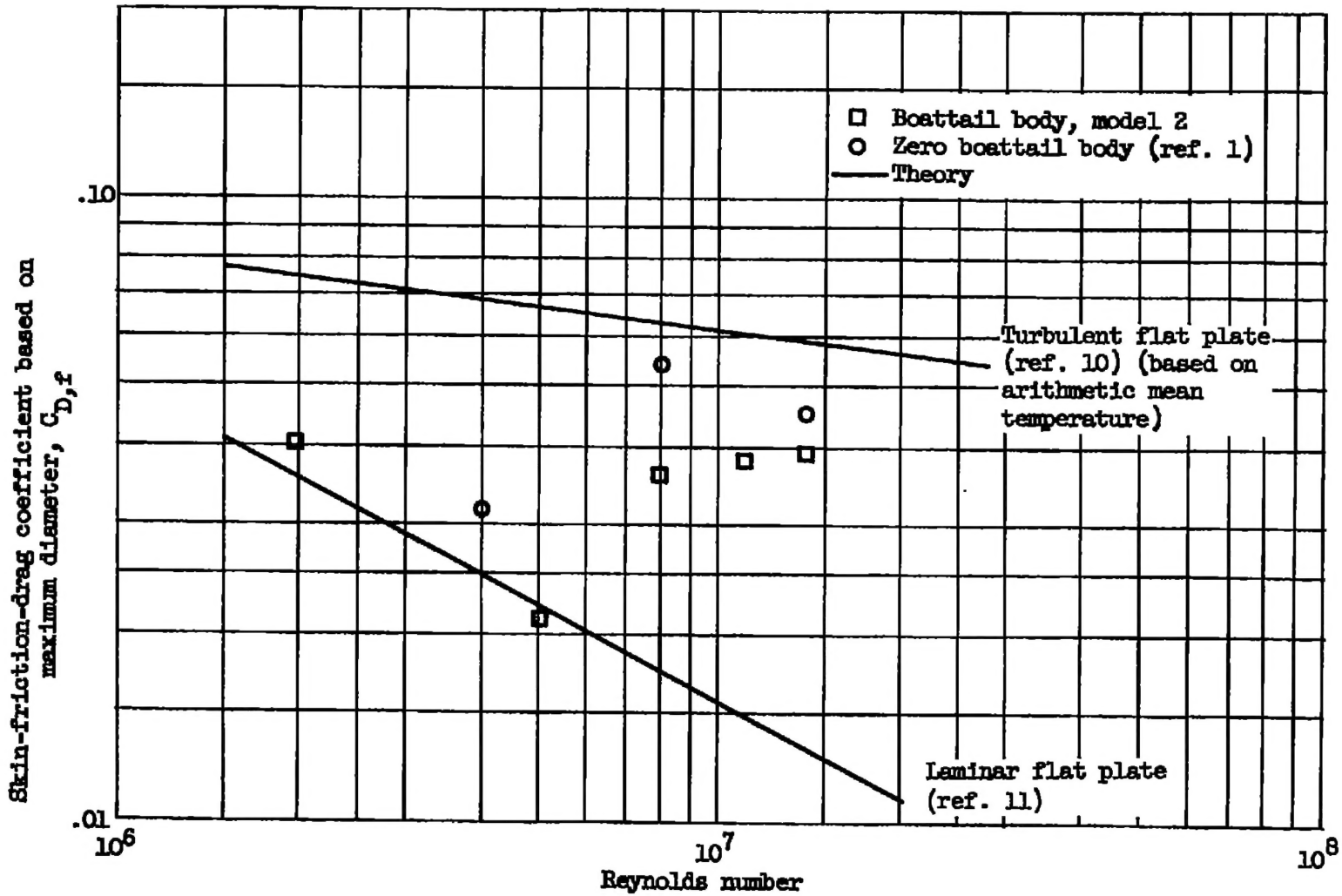

Figure 10. - Comparison of skin-friction drag between boattailed model 2 and zero boattailed body of reference 1.

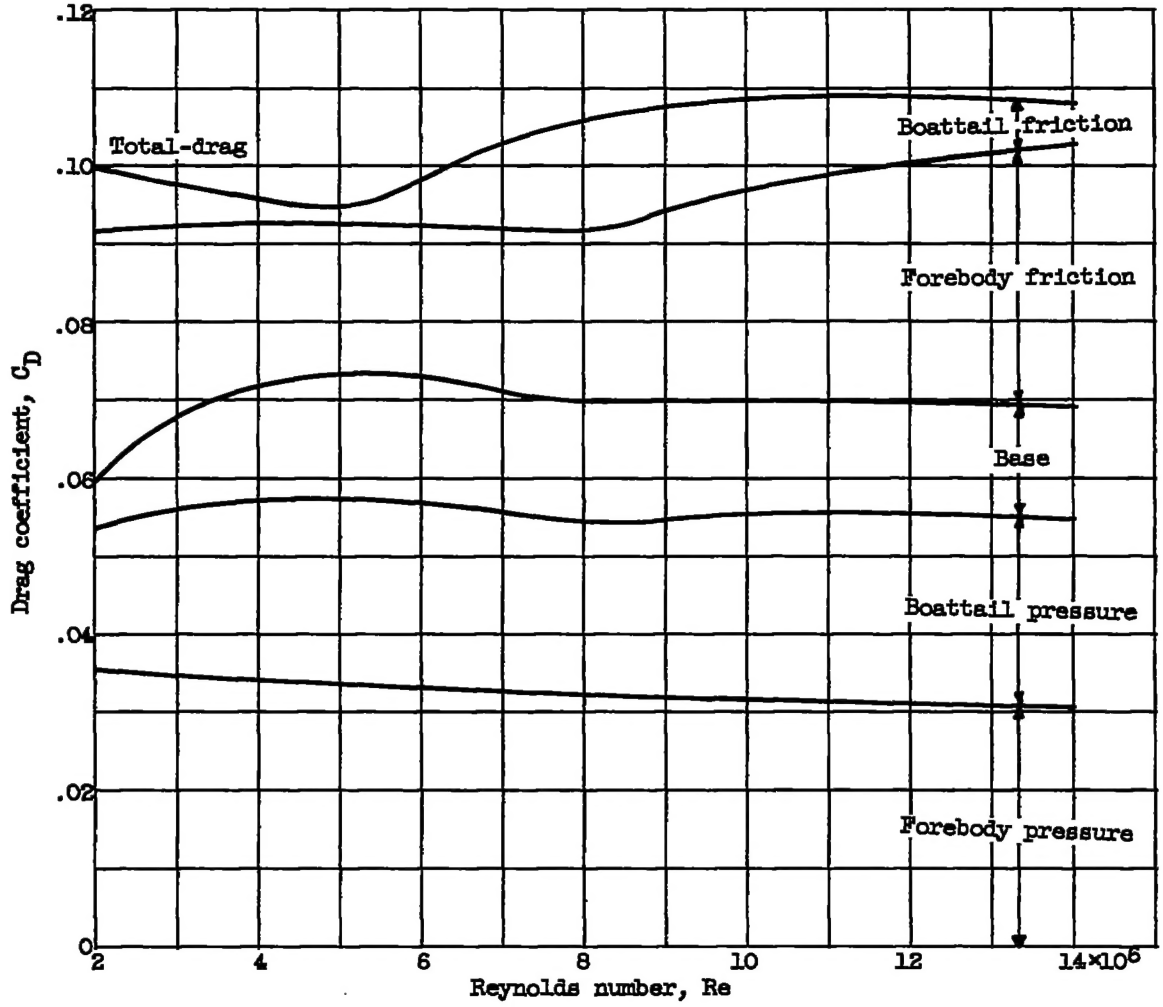

Figure 11. - Variation of total and component drag coefficients with Reynolds number for zero angle of attack.

NACA-Langley - 5-6-54 - 350